

High Resolution Photoemission Study on Low- T_K Ce Systems: Kondo Resonance, Crystal Field Structures, and their Temperature Dependence

D. Ehm and S. Hüfner

Universität des Saarlandes, Fachrichtung 7.2 — Experimentalphysik, 66041 Saarbrücken, Germany

F. Reinert*

Experimentelle Physik II, Universität Würzburg, D-97074 Würzburg, Germany

J. Kroha

Physikalisches Institut, Universität Bonn, Nussallee 12, D-53115 Bonn, Germany

P. Wölfle

Institut für Theorie der Kondensierten Materie, Universität Karlsruhe, Engesserstr. 7, D-76128 Karlsruhe, Germany

O. Stockert and C. Geibel

Max-Planck Institute for Chemical Physics of Solids, Nöthnitzer Str. 40, 01187 Dresden, Germany

H. von Löhneysen

Physikalisches Institut, Universität Karlsruhe, D-76128 Karlsruhe, Germany

(Dated: October 7, 2018)

We present a high-resolution photoemission study on the strongly correlated Ce-compounds CeCu₆, CeCu₂Si₂, CeRu₂Si₂, CeNi₂Ge₂, and CeSi₂. Using a normalization procedure based on a division by the Fermi-Dirac distribution we get access to the spectral density of states up to an energy of $5k_B T$ above the Fermi energy E_F . Thus we can resolve the Kondo resonance and the crystal field (CF) fine-structure for different temperatures above and around the Kondo temperature T_K . The CF peaks are identified with multiple Kondo resonances within the multiorbital Anderson impurity model. Our theoretical $4f$ spectra, calculated from an extended non-crossing approximation (NCA), describe consistently the observed photoemission features and their temperature dependence. By fitting the NCA spectra to the experimental data and extrapolating the former to low temperatures, T_K can be extracted quantitatively. The resulting values for T_K and the crystal field energies are in excellent agreement with the results from bulk sensitive measurements, e.g. inelastic neutron scattering.

PACS numbers: 71.27.+a 71.28.+d 79.60.-i 71.10.-w

I. INTRODUCTION

Since the experimental discovery of heavy-fermion (HF) compounds, metallic systems with rare-earth ($4f$) and actinide ($5f$) elements have been thoroughly investigated both experimentally and theoretically.^{1,2} The term heavy-fermions refers to the observation that these systems behave as if the conduction electrons had an enormously high effective mass. The coefficient of the linear term in the low-temperature specific heat, the Sommerfeld coefficient, can be of the order of $1 \text{ JK}^{-2} \text{ mol}^{-1}$, corresponding to an effective electron mass enhancement of a factor 1000 compared to the free electron mass. In addition, these $4f$ and $5f$ systems show a variety of anomalous ground state and unusual low-temperature properties.^{3,4}

The single-impurity Anderson model⁵ (SIAM) embodies the key mechanisms of the many-body physics in heavy-fermion systems, namely a strong local Coulomb interaction of the f -electrons with the resulting local moment formation and a weak hybridization between conduction electron states and f states, which lead to the

Kondo effect.^{6,7} For cerium systems the theoretical description is significantly simplified, because the Ce ions contain at most only one $4f$ -electron (i.e. $4f^1$). Employing variational methods^{8,9}, numerical renormalization group (NRG) calculations^{10,11} or self-consistent diagrammatic resummations, like the non-crossing approximation (NCA)^{11,12} and the conserving T -matrix approximation (CTMA)^{13,14,15}, one can calculate the f spectral density of states (DOS) near the Fermi level within the framework of the SIAM. The most important feature in the $4f$ DOS of Ce-systems is a narrow peak with a maximum just above the Fermi Energy E_F , the *Kondo resonance*. The line width of the Kondo-resonance is given by the low-energy scale of the problem, defined by the Kondo-temperature T_K . For Ce systems $k_B T_K$ is typically a few meV, although the bare model parameters of the SIAM are usually two or three orders of magnitude larger.

Although in the HF compounds the f -atoms form an ordered lattice, the simplest approach is the SIAM, employing non-interacting local impurities, which has been very successful in even a quantitative description of high-

resolution photoemission spectra¹⁶. This can be understood as follows: The direct orbital overlap between adjacent f -atoms is negligible, so that the on-site Kondo resonances form coherent delocalized states below the lattice coherence temperature only due to their coupling via the conduction band. Therefore, their dispersion band width is essentially given by the Kondo resonance width itself, i.e. by the single-impurity Kondo temperature T_K . Since photoemission spectroscopy (PES) measures predominantly the momentum integrated f -spectra, these PES spectra are well described by the SIAM. However, to describe the coherent heavy-fermion state with a dispersing narrow band close to the Fermi level, other models like the renormalized band picture¹⁷ or the periodic Anderson model (PAM)¹⁸ are required.

PES, in particular angle resolved photoelectron spectroscopy with excitation energies in the VUV-range (ARUPS), is one of the most direct experimental methods to investigate the electronic structure of solids. For rare-earth systems, PES allows to study the occupied part of the $4f$ spectral function with high accuracy. Unfortunately, the main spectral weight of the Kondo resonance appears above the Fermi level, where the photoelectron intensity is suppressed by the Fermi-Dirac distribution (FDD). On the other hand, *inverse* PES (IPES) can in principle measure the density of states *above* E_F , but the energy resolution — usually considerably larger than 100 meV — is not sufficient to investigate the details of the interesting $4f$ spectral features, i.e. the Kondo resonance, the crystal field structures (CF), and in most cases even not the spin-orbit splitting. Recently it has been shown¹⁹ on CeCu₂Si₂ that PES with high energy resolution gives access to the Kondo resonance (KR). This first and direct observation of the KR was possible by the application of a well known normalization procedure²⁰ that allows to recover the thermally occupied DOS up to $\sim 5k_B T$ above E_F . At higher temperatures this energy range can even cover the CF structures above the KR. From the normalized PES data one can determine the Kondo temperature T_K from the KR line width and the CF splittings of the $J = 5/2$ spin-orbit partner (Δ_{CF}). A more detailed quantitative analysis is possible by comparing the experimental $4f$ spectrum with theoretical spectral functions calculated by the *non crossing approximation* (NCA).¹⁶ By iteratively fitting the data one can determine all relevant model parameters of the SIAM,²¹ from which eventually T_K and Δ_{CF} can be extracted.

In this paper we present a systematic investigation of the classical HF systems CeCu₆, CeCu₂Si₂, CeRu₂Si₂, CeNi₂Ge₂, and CeSi₂, which show Kondo temperatures from 5 K to about 40 K as extracted from other experiments. As explained later, we restrict our investigations to γ -Ce like materials showing a low hybridization strength and consequently low Kondo temperatures. We compare the PES results for the Kondo temperatures and the crystal field energies with values determined by bulk sensitive measurements.

The manuscript is organized as follows: after a description of the SIAM, we explain the individual features in the $4f$ density of states and aspects of the numerical NCA calculations (Sec. II). In section III following section, we describe the experimental setup and the sample preparation. Section IV gives the experimental and theoretical results for the different HF compounds, followed by a discussion of the quantitative analysis. Finally, in the appendix we explain in detail the normalization method and the modeling of the spectra.

II. THEORY OF THE SPECTRAL FEATURES

The SIAM Hamiltonian for Ce in a metallic host reads,

$$H = H_0 + \sum_{m\sigma} \varepsilon_{fm} f_{m\sigma}^\dagger f_{m\sigma} + \sum_{\mathbf{p}\sigma} [V_{\mathbf{p}m} f_{m\sigma}^\dagger c_{\mathbf{p}\sigma} + h.c.] + \frac{U}{2} \sum_{(m\sigma) \neq (m'\sigma')} f_{m\sigma}^\dagger f_{m\sigma} f_{m'\sigma'}^\dagger f_{m'\sigma'}, \quad (1)$$

where $H_0 = \sum_{\mathbf{p}\sigma} \varepsilon_{\mathbf{p}} c_{\mathbf{p}\sigma}^\dagger c_{\mathbf{p}\sigma}$ describes the conduction electron band, and $f_{m\sigma}^\dagger$ creates an electron with spin σ in a $4f$ -orbital with energy $\varepsilon_{fm} < E_F$, $m = 1, \dots, 2S$, $S = 7/2$. The $4f$ -orbitals hybridize with the conduction band via the matrix elements $V_{\mathbf{p}m}$. For later use we introduce the effective couplings $\Gamma_{mm'} = \pi \sum_{\mathbf{p}} V_{m\mathbf{p}}^* V_{\mathbf{p}m'} A_{\mathbf{p}\sigma}(0) < |\varepsilon_{fm}|$, with $A_{\mathbf{p}\sigma}(\omega)$ the conduction electron spectral function and $N(\omega) = \sum_{\mathbf{p}} A_{\mathbf{p}\sigma}(\omega)$ the conduction electron density of states per spin, which in the following will be assumed to be flat. The Coulomb repulsion U between electrons in any of the local orbitals is large enough to suppress any double occupancy of the $4f$ -shell and may be assumed $U \rightarrow \infty$ in the following. For the quantum mechanical treatment of spin as well as charge fluctuations the f -electron operators can then be represented as $f_{m\sigma}^\dagger = g_{m\sigma}^\dagger b$, where the bosonic and fermionic auxiliary operators, b^\dagger , $g_{m\sigma}^\dagger$, create the empty and the singly occupied f -shell ($m\sigma$), respectively, and obey the constraint,

$$\hat{Q} = \sum_{m\sigma} g_{m\sigma}^\dagger g_{m\sigma} + b^\dagger b = 1. \quad (2)$$

The spectrum of this system has generically six distinct features as shown in Fig. 1 (A–F). They can be understood as follows: At low T the occupation of the lowest $4f$ level is close to unity, $n_{f1} \lesssim 1$, while all other $4f$ orbitals are essentially empty, $n_{fm} \approx 0$, $m = 2, \dots, 7$. Hence, the broad $4f^1 \rightarrow 4f^0$ ionization peak (A) with a full width at half maximum (FWHM) of $\Gamma \approx \sum_m \Gamma_{1m}$ corresponds to the lowest single-particle level ε_{f1} . Resonant spin flip scattering of electrons at the Fermi energy induces the narrow Kondo resonance (D) of width $\sim k_B T_K$, shifted by $\delta \approx \sin(\pi n_{f1}) k_B T_K$ above E_F due to level repulsion from the single-particle levels ε_{fm} (see Ref. 22 for details). The spin-orbit (SO) and the crystal field (CF) peaks appear in pairs (B, F) and (C, E), respectively. They arise from virtual transitions from the

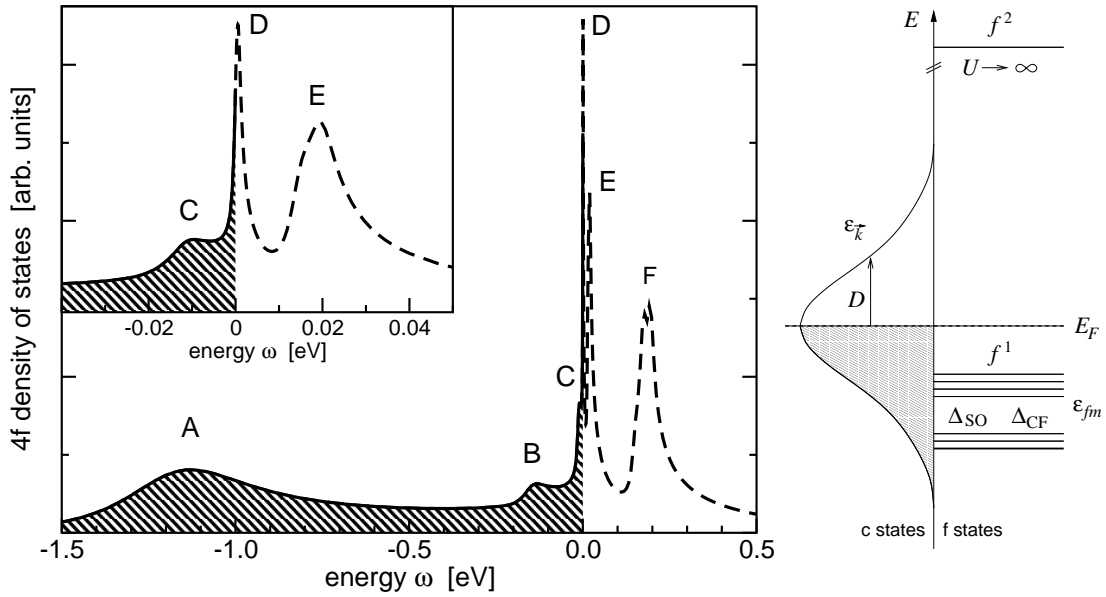


FIG. 1: Left: Theoretical $4f$ spectrum from NCA calculations based on the SIAM for $T = 11$ K and the model parameters given in the captions of Fig. 5. The hatched region indicates the 'photoemission' region below E_F . The inset shows the near- E_F region with Kondo resonance (D) and crystal field features (C,E). B and F are the spin-orbit satellites ($J = 5/2$), A is the ionization peak. For finite U the two-electron state f^2 would appear far right of the displayed energy range at $\approx U - |\epsilon_f|$. Right: Sketch of the energy level scheme of the SIAM for the conduction band states (c states) and for the impurity (f -states).

ground state into the (empty) excited SO (F) and CF (E) states and vice versa (B and C). The positions of the satellite peak pairs are, therefore, approximately symmetrical about the central Kondo peak (D). However, while the features above E_F have significant spectral weight, those below E_F appear merely as weak shoulders. This is because the transition probabilities carry a detailed balance factor $w = n^i(1 - n^f)$, where n^i (n^f) is the occupation number of the $4f$ orbital in the initial (final) state, i.e. w is large for the excitations E, F, but small for the transitions B, C. As n^i and n^f are controlled both by quantum and thermal fluctuations the CF and SO satellites are T -dependent and are signatures of strong correlations.

We now analyze the nature of the satellite peaks in more detail. A straight-forward Schrieffer-Wolff projection onto the subspace of the singly occupied $4f$ -shell yields an $s - d$ exchange model, generalized to multiple local levels,

$$H_{sd} = H_0 + \sum_{m\sigma} \epsilon_{fm} g_{m\sigma}^\dagger g_{m\sigma} + \sum_{\mathbf{p}\mathbf{p}'mm'} \sum_{\substack{\sigma_1\sigma_2\sigma_3\sigma_4 \\ \sigma_1+\sigma_3=\sigma_2+\sigma_4}} J_{mm'} c_{\mathbf{p}\sigma_1}^\dagger c_{\mathbf{p}'\sigma_2} g_{m\sigma_3}^\dagger g_{m'\sigma_4}, \quad (3)$$

subject to the constraint (2) with vanishing boson number. The effective spin exchange couplings, including level renormalizations to second order in $V_{\mathbf{p}m}$ (for non-

degenerate levels), are obtained as,¹⁶

$$J_{mm'} = \frac{\sum_{\mathbf{p}} V_{m\mathbf{p}}^* V_{\mathbf{p}m'}}{\left| \epsilon_{f1} + \sum_{n>1} \frac{|\sum_{\mathbf{p}} V_{\mathbf{p}n}|^2}{\epsilon_{fn} - \epsilon_{f1}} \right|}. \quad (4)$$

Due to the anti-commutative operator structure of the spin coupling term in the Hamiltonian (3) the conduction electron-local spin T-matrix acquires in second order perturbation theory in the J s logarithmic divergences at the transition energies between the local levels, $\omega = \epsilon_{fn} - \epsilon_{fm}$,

$$T_{mm'}(\omega, T) = -N(0) \sum_n J_{mn} J_{nm'} \times \ln \left| \frac{(\omega + \epsilon_m - \epsilon_n)^2 + \pi T^2}{D^2} \right|. \quad (5)$$

This expression is derived in a straight-forward way using the bare auxiliary fermion propagator $G_{m\sigma}^{(0)}(\nu) = (\nu - \lambda - \epsilon_m)^{-1}$, where the parameter λ is taken to infinity to project onto the constrained Hilbert space of single occupancy of the $4f$ -shell (see e.g. Ref. 11). m and m' denote which of the $4f$ -orbitals is occupied in the incoming and in the outgoing channel, respectively, ω is the energy of the scattering conduction electron, and the incoming local particle is assumed to be at the eigenenergy of the initial orbital, ϵ_{fm} (on-shell). Due to the detailed balance factors mentioned above, the divergencies in Eq. (6) give a significant contribution to the $4f$ spectral density only, if at least one of the levels m or

n is the local ground state. The logarithmic energy and temperature dependence demonstrates that the SO and CF satellite peaks are, in fact, Kondo resonances, i.e. induced by quantum spin flip processes, however shifted by the excitation energies $\omega = \pm(\varepsilon_{fm} - \varepsilon_{f1})$ with respect to the central Kondo peak near $\omega = 0$. Despite these multiple Kondo peaks a single Kondo temperature T_K is defined as the crossover scale below which the collective spin singlet ground state is formed. Since at temperatures below the SO and CF splitting energies only the $4f$ ground state level ε_{f1} is significantly occupied, it may be estimated as,¹⁶

$$T_K \approx \sqrt{2J_{00}E_F} e^{-1/(2N(0)J_{00})} \quad (6)$$

and is, hence, given by the width of the *central* Kondo peak near the Fermi energy (D in Fig. 1). The phonon-induced broadening of the Kondo resonance and its satellites is not considered here, because the coupling of the phonons to the spin excitations is small. A detailed analysis of the spectral weights and widths of the multiple resonances will be given elsewhere, see also Ref. 23.

The self-consistent NCA equations are formulated in terms of the auxiliary fermion and boson propagators G_f , G_b ,

$$[G_\sigma^{-1}]_{mm'}(\nu) = (\nu - \lambda - \varepsilon_{fm})\delta_{mm'} - \Sigma_{g\sigma mm'}(\nu) \quad (7)$$

$$B^{-1}(\nu) = \nu - \lambda - \varepsilon_{fm} - \Sigma_b(\nu), \quad (8)$$

where the auxiliary fermion selfenergy Σ_g is a matrix in orbital space because of the non-conservation of the orbital degree of freedom m , $\delta_{mm'}$ denotes the Kronecker delta and the superscript -1 matrix inversion. In NCA the selfenergies Σ_g , Σ_b and the physical $4f$ spectral function A_f are given by,

$$\Sigma_{g\sigma mm'}(\nu) = \Gamma_{mm'} \int d\varepsilon [1 - f(\varepsilon)] N_\sigma(\varepsilon) B(\nu - \varepsilon) \quad (9)$$

$$\Sigma_b(\nu) = \sum_{\sigma mm'} \Gamma_{mm'} \int d\varepsilon f(\varepsilon) N_\sigma(\varepsilon) G_{\sigma mm'}(\nu + \varepsilon) \quad (10)$$

$$A_{f\sigma mm'}(\omega) = \int d\varepsilon e^{-\beta\varepsilon} [A_{g\sigma mm'}(\omega + \varepsilon) A_b(\varepsilon) + A_{g\sigma mm'}(\varepsilon) A_b(\varepsilon - \omega)] \quad (11)$$

where all propagators are understood as the retarded ones, and the spectral functions are $A_g(\nu) = -\text{Im}G(\nu)/\pi$, etc. See Refs. 11, 15 for the exact projection onto the physical Hilbert space of no multiple $4f$ -shell occupation and for an efficient numerical evaluation of the NCA equations.

The NCA is known to correctly include the logarithmic perturbative corrections in the absence of a magnetic field^{22,24} and to reproduce the correct Kondo peak width,¹¹ as long as the temperature is not too far below T_K . It may also be shown to incorporate the above-mentioned detailed balance factors and, hence, describes well the spectral features discussed above (Fig. 2).

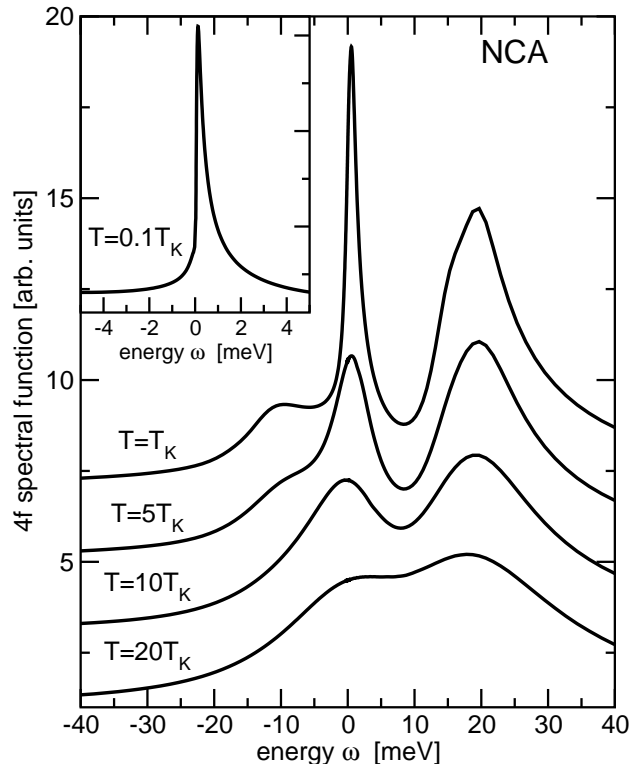


FIG. 2: Theoretical $4f$ spectrum from NCA calculations based on SIAM for different temperatures. The displayed energy range covers the Kondo resonance close to zero and the crystal field structures at approx. -10 meV and $+20$ meV. The inset shows the Kondo resonance at low temperatures, i.e. at $T = 0.1T_K$ (unitarity limit).

In order to estimate T_K of the experimental results by fitting of the NCA spectra, one calculates the respective NCA spectra at $T = 0.1T_K \approx 1$ K, i.e. close to the unitarity limit. T_K can then be determined from the peak width of this theoretical low- T spectrum (see inset of Fig. 2). As already seen in Fig. 1 at low T , i.e. $T \approx T_K$, the central KR appears as a narrow line, well separated from the CF satellites above and below the Fermi level. Towards higher temperatures, the line width of the KR increases, while the maximum intensity becomes smaller and the distinction of the KR and the CF features is successively smeared out. At $T \gg T_K$ the KR disappears as separate peak and an enhanced $4f$ density of states (DOS) near E_F is rather due to the CF excitations. Thus, the persistence of an enhanced DOS at the Fermi level even at high T in comparison to T_K is naturally explained within the SIAM in combination with CF excited states and their logarithmically wide extension towards high T .

III. EXPERIMENTAL SETUP

The PES experiments have been performed with a SCIENTIA SES 200 analyzer in combination with a

monochromatized GAMMADATA VUV lamp at photon energies of $h\nu = 21.23$ eV (He I $_{\alpha}$) and $h\nu = 40.8$ eV (He II $_{\alpha}$). The base pressure of the UHV system was below 5×10^{-11} mbar, increasing during the measurements — due to the He leakage from the discharge lamp — to $\lesssim 1 \times 10^{-9}$ mbar. The samples could be cooled down to approximately $T = 4$ K on the manipulator in the spectrometer chamber. For the presented data analysis the calibration of the spectrometer is very crucial, in particular the sample (surface) temperature, the energy resolution, and the position of the Fermi level. For this purpose we have repeatedly performed low-temperature reference measurements on polycrystalline Ag and on polycrystalline Nb in the superconducting state. By an analysis of these data one can independently determine the required parameters.^{25,26} For the measurements presented here the energy resolution of the spectrometer was chosen to 5.4 meV as a compromise between intensity — in particular when using He II $_{\alpha}$ radiation — and energy resolution. More about the spectrometer can be found in Ref. 27

A. Sample preparation

The five different Ce compounds investigated in this work belong to the class of HF compounds which are characterized by large specific heat coefficients γ_0 . Whereas CeCu $_6$ displays with $\gamma_0 = 1.6$ JK $^{-2}$ mol $^{-1}$ the largest value²⁸ among the investigated compounds, the other systems range from $\gamma_0 = 1.1$ JK $^{-2}$ mol $^{-1}$ for CeCu $_2$ Si $_2$ ^{29,30} down to $\gamma_0 = 0.104$ JK $^{-2}$ mol $^{-1}$ for CeSi $_2$.³¹ (CeRu $_2$ Si $_2$ ³² and CeNi $_2$ Ge $_2$ ³³: $\gamma_0 = 350$ mJK $^{-2}$ mol $^{-1}$). None of these compounds shows any magnetic order down to temperatures of a few mK.^{2,33,34,35,36,37,38,39} In the case of CeCu $_2$ Si $_2$ and CeNi $_2$ Ge $_2$ there is a superconducting phase transition at $T_c = 0.5$ K 2 and 0.1 K 40 , respectively.

The single-crystalline CeCu $_6$ samples were grown by Czochralski technique in a high-purity argon atmosphere using a tungsten crucible. In contrast to this the polycrystals CeSi $_2$, CeCu $_2$ Si $_2$, CeRu $_2$ Si $_2$, and CeNi $_2$ Ge $_2$ were produced by first melting the respective stoichiometric ingredients also under high-purity argon atmosphere and then tempering in a dynamic vacuum. The purity of the used elements amounts to 99.99 % at least. The temperature and the duration of the temper process varies from system to system between 800–1200°C and 50–120 hours. All these compounds were characterized as single phase compounds by the use of x-ray diffraction technique, that also yields the crystal structure and lattice parameters. Whereas all the ternary compounds crystallize in the tetragonal ThCr $_2$ Si $_2$ -structure^{41,42,43} with lattice constants $a = 4.10$ Å, 4.20 Å, and 4.15 Å, and $c = 9.93$ Å, 9.80 Å, and 9.85 Å for CeCu $_2$ Si $_2$, CeRu $_2$ Si $_2$, and CeNi $_2$ Ge $_2$, respectively, CeSi $_2$ crystallizes in the tetragonal α -ThSi $_2$ -structure⁴⁴ with $a = 4.19$ Å and $c = 13.91$ Å. The crystal structure of CeCu $_6$ under-

goes a change from orthorhombic symmetry at temperatures above 200 K to monoclinic at low temperatures.⁴⁵ Because the following investigations on this compound have all be done in the monoclinic phase, only the lattice parameters for this structure are given: $a = 5.08$ Å, $b = 10.12$ Å, $c = 8.07$ Å, and $\beta = 91.36^\circ$.

To prepare clean surfaces the samples, cut to a typical size of $2 \times 3 \times 5$ mm 3 and equipped with a cleavage post, were fractured *in situ* at low temperatures just before the UPS measurement. The resulting surfaces were usually coarse grained, even when the sample was single crystalline. In the latter case, the rough surface topology ensures an integration over a sufficiently large effective k -space. This is important, because a strong angular dependence of the $4f$ intensity was observed.^{46,47} Scraping the surface with a diamond file did not yield satisfying results.⁴⁸ Because of the high surface reactivity of the rare-earth compounds the duration of the measurement was kept below 12 h. During this period the surface quality was repeatedly checked by a measurement of the O $2p$ photoemission intensity at binding energies of about 6 eV in the valence band spectra.

IV. RESULTS AND DISCUSSION

In the following section we present our results on five HF compounds with Kondo temperatures below 100 K, namely CeCu $_6$ ($T_K = 5$ K⁴⁹), CeCu $_2$ Si $_2$ (10 K⁵⁰), CeRu $_2$ Si $_2$ (20 K⁴⁹), CeNi $_2$ Ge $_2$ (30 K³³), (41 K⁵¹); the given Kondo temperatures T_K are determined by inelastic neutron scattering (INS). Here we restrict our investigations to low- T_K or γ -Ce like materials with a low hybridization strength because of two reasons: First it is a well known fact that these γ -like materials only exhibit a small change in hybridization strength by going from the bulk to the surface that is not the case in α -like Ce compounds.⁵² Recently J. W. Allen⁵³ showed that PE spectra of γ -like Ce compounds mostly exhibit bulk rather than surface contributions. Second, the position of the KR in heavy fermion Ce compounds occurs above E_F at $\delta \approx \sin(\pi n_{f1})k_B T_K$.²² Because our normalization method (described in detail in Appendix A) only allows to observe spectral features in the energy range between E_F and $5k_B T$ above E_F , it is a crucial aspect to find the KR in this energy interval at low temperature. By using the normalization procedure we are also able to compare the PE spectra with NCA spectral functions. To get a quantitative comparison, we have to apply this normalization method to both the PES data and the NCA results. By the performance of a conventional χ^2 -fitting procedure, we get a suitable parameter set for the description of the spectral function of Ce systems as described in Sec. II.

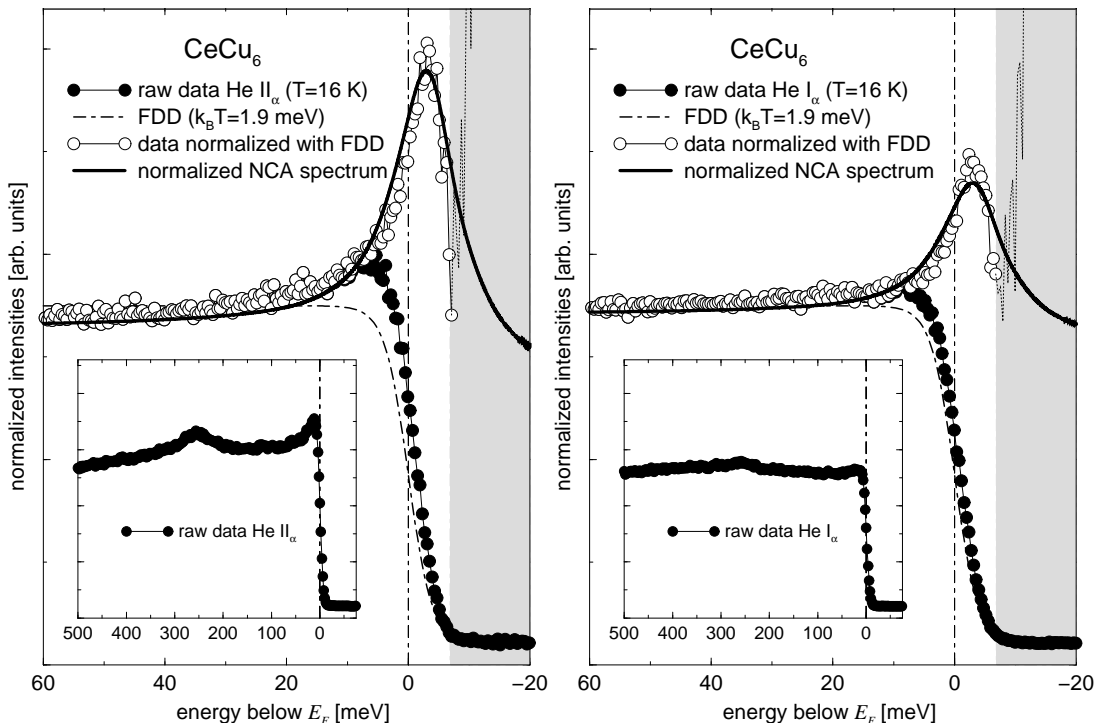


FIG. 3: Photoemission spectrum of CeCu_6 (left panel: He II_α with $h\nu = 40.8$ eV; right panel: He I_α with $h\nu = 21.2$ eV). Filled circles represent the raw data ($\Delta E = 5.4$ meV, $T = 16$ K), mainly consisting of the tail of the KR. The SO partner ($J = 7/2$) appears at a higher binding energy of ≈ 250 meV given in the inset ($\Delta E \approx 15$ meV). Open circles represent the normalized data using the experimentally broadened FDD, the shaded area marks the unreliable spectral range above $5k_B T$. The solid line represents the fitted NCA spectral function with $\epsilon_f = -1.05$ eV, $D = 2.8$ eV, CF splittings of the $J = 5/2$ sextet $\Delta_{CF} = 7.2/13.9$ meV, SO splitting $\Delta_{SO} = 250$ meV, hybridization $V = 116$ meV.

	from other experiments			from PES		
	T_K [K]	CF [meV]		T_K [K]	CF [meV]	
		$\Delta_{1 \rightarrow 2}$	$\Delta_{1 \rightarrow 3}$		$\Delta_{1 \rightarrow 2}$	$\Delta_{1 \rightarrow 3}$
CeCu_6	$5.0 \pm 0.5^{(a)49}$	$7.0^{(a)54}$	$13.8^{(a)54}$	4.6	7.2	13.9
CeCu_2Si_2	$4.5^{(b)55} - 10^{(a)50}$	$30^{(a)54} - 36^{(c)56}$	—	6	32	37
CeRu_2Si_2	$16^{(a)57}$	$19^{(d)58}$	$34^{(d)58}$	16.5	18	33
CeNi_2Ge_2	$29^{(a)33}$	$(4)^{(a)59}$	$34^{(a)59}$	29.5	26	39
CeSi_2	$22/41^{(a)51}$	$25^{(a)51}$	$48^{(a)51}$	35	25	48

TABLE I: Comparison of the Kondo temperatures T_K and the CF energies Δ_{CF} determined from PES and from other experimental methods, namely from (a): INS studies, (b): specific heat measurements, (c): Raman scattering experiments, and (d): theoretical considerations based on specific heat measurements.

A. Low-temperature spectra of CeCu_6

The first presented system is the prototype HF compound CeCu_6 . Because of the small Kondo-temperature of only $T_K \approx 5$ K and the correspondingly weak $4f$ spectral weight at the Fermi level, there exist only few valence

band photoemission studies on this compound.^{60,61,62,63} Our high resolution photoemission spectra on CeCu_6 are displayed in Fig. 3 measured at $T = 16$ K with both He I_α (right panel) and He II_α (left panel) radiation. The insets show an extended energy range below E_F over 500 meV with the weak tail of the Kondo resonance at E_F and the

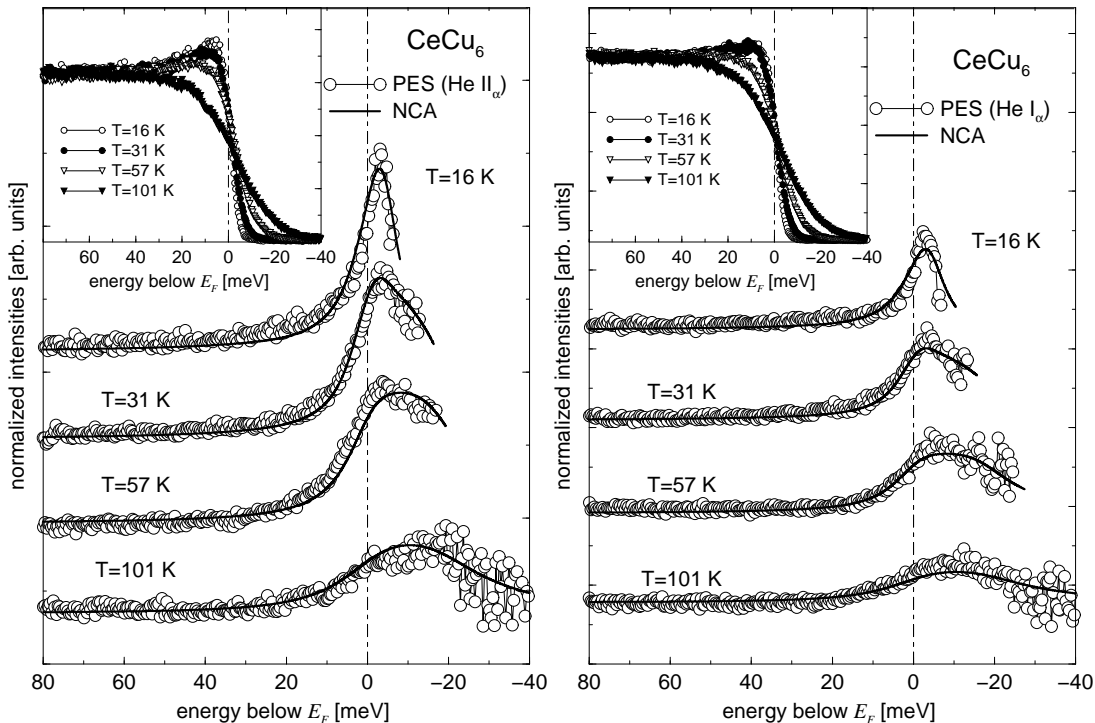


FIG. 4: Temperature dependence of the experimental (PES) and calculated $4f$ spectra of CeCu_6 after the application of the normalization procedure. The PES data are taken with He II_α (left panel) and He I_α radiation (right panel). The used NCA model parameters are given in the caption of Fig. 3. The insets show the raw spectra, normalized to the same intensity at a binding energy of ≈ 100 meV.

SO feature at approx. 260 meV corresponding to peak B in Fig. 1. Although the photoionization cross section of the Ce $4f$ states increases about a factor 3.2 from an excitation energy of $h\nu = 21.23$ eV to 40.8 eV⁶⁴ both spectra clearly reveal the $4f$ derived spectral features over the conduction band background, although the $4f$ intensity with He I is significantly reduced.

In the blowup of the near- E_F region in Fig. 3, only the tail of the KR is discernible, with an increasing intensity towards E_F . The spectral information above the Fermi level — the maximum intensity of the Kondo resonance is anticipated slightly above E_F — is suppressed by the Fermi-Dirac distribution (FDD) that steeply goes to zero for small temperatures. The spectral information can partly be restored when the above mentioned normalization method (see Appendix A) is applied to the raw He data. As demonstrated already for He II-data on CeCu_2Si_2 in Ref. 16, there appears obviously a narrow peak with a full width at half maximum (FWHM) of ≈ 6 meV and a maximum at about 3 meV above E_F . The peak can be observed in both the He II $_\alpha$ and in the He I $_\alpha$ spectra, but with a peak-to-background intensity ratio which is about a factor of 2 larger for He II. The peak maximum is sufficiently below the upper limit of $5k_B T \approx 7$ meV for the applicability of the method $5k_B T \approx 7$ meV, where the noise of the data becomes enormously magnified due to the exponential decrease of

the FDD. It should be mentioned that the data for binding energies below $2k_B T$ (below E_F) remain unchanged by the normalization procedure.

In order to analyze the narrow peak feature further, we have performed NCA calculations with a set of model parameters that is given in the figure caption of Fig. 3. The starting points for the model parameters are taken from the photoemission spectra at higher energies (ϵ_f , Δ_{SO}) or from other experiments, as e.g. inelastic neutron scattering (Δ_{CF}), and then reasonably modified to fit the normalized experimental spectra. The intensity ratio between $4f$ and conduction band states, which are assumed to be constant in energy, is set arbitrarily, the Coulomb energy U is infinite. The agreement between theory and experiment is striking. The NCA result is able to describe exactly the experimental line shape and the energetic position of the narrow peak just above E_F both in the spectra taken with He II $_\alpha$ and He I $_\alpha$ radiation.

B. Temperature dependence of the CeCu_6 $4f$ spectra

The NCA allows to calculate spectra for finite temperatures. All physical properties — and in particular the spectral density of states¹² — scale with the Kondo

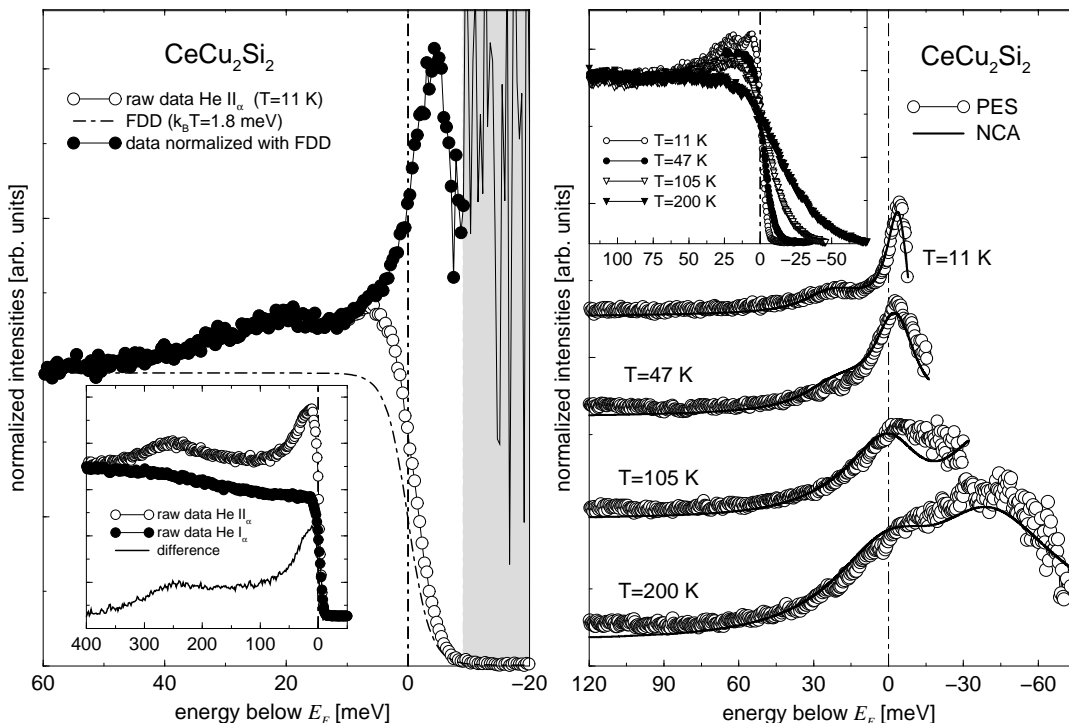


FIG. 5: Photoemission spectra of CeCu_2Si_2 (He II_α , $h\nu = 40.8$ eV). Left panel: normalization at $T = 11$ K (cf. Fig. 3); the inset shows an extended energy range ($\Delta E \approx 15$ meV) including the SO ($J = 7/2$) excitation at ≈ 270 meV below E_F taken with He II_α radiation (open circles) and with He I_α (filled circles). Right panel: temperature dependence of the experimental (He II_α) and the calculated $4f$ spectral function of CeCu_2Si_2 after the normalization. Model parameters: $\epsilon_f = -1.57$ eV, $D = 4.3$ eV, $\Delta_{CF} = 32/37$ meV, $\Delta_{SO} = 270$ meV, $V = 200$ meV. The inset shows the raw data normalized to the same intensity at a binding energy of ≈ 100 meV.

temperature T_K . In addition, the recoverable energy range (above E_F) increases linearly with T , because the thermal broadening of the FDD increases with the sample temperature. Therefore we analyzed the near- E_F spectral structures of CeCu_6 for different temperatures. Fig. 4 shows the experimental data plus the NCA result at several temperatures, normalized at the FDD at the respective temperature (see Appendix A). Again we applied the normalization to both the He II_α (left panel) and the He I_α (right panel) spectra on CeCu_6 . The insets give the raw data, normalized at the same intensity at $E_B = 100$ meV. These data are dominated by the increasing broadening of the FDD and the vanishing tail of the Kondo resonance.

As already seen in Fig. 3 at low T , the KR appears in the recovered data at $T = 16$ K as a narrow line just above E_F . Towards higher temperatures the line width of the KR increases while the maximum intensity becomes smaller. The spectra of systems which clearly resolve a crystal field (CF) structure (see below CeCu_2Si_2 and CeNi_2Ge_2) show an additional smearing of the crystal field fine structure. At $T = 101$ K and above, the narrow peak of the KR has disappeared, and is replaced by a broad structure with a maximum at ≈ 10 meV above E_F , which results in a considerable $4f$ density of states

right at the Fermi level.

With the same model parameters as for the low-temperature spectrum in Fig. 3 we have calculated the spectra at the higher experimental temperatures. The temperature dependence observed in the experimental data is perfectly reproduced by the NCA result which is qualitatively described in Fig. 2. As we will discuss further below, the existence of the crystal field splittings of the $4f$ levels has a considerable influence on the distribution of spectral weight near the Fermi level.

C. CeCu_2Si_2 , CeRu_2Si_2 , CeNi_2Ge_2 , CeSi_2 : Low- T spectra and temperature dependence

This becomes more clear in the case of the HF-compound CeCu_2Si_2 with a Kondo temperature of $T_K \approx 10$ K and a crystal field energy of about 30 meV (see references given in Tab. I). At $E_B \approx 20$ meV the raw low-temperature spectra show a clearly distinct crystal-field structure in the $4f_{5/2}$ levels.⁵⁴ A similar CF structure could also be observed in CeB_6 ⁶⁵ and is also visible in the CeNi_2Ge_2 spectra below. In addition to this fine structure, the high-temperature data show a large shift of the broad peak maximum to approx. 45 meV

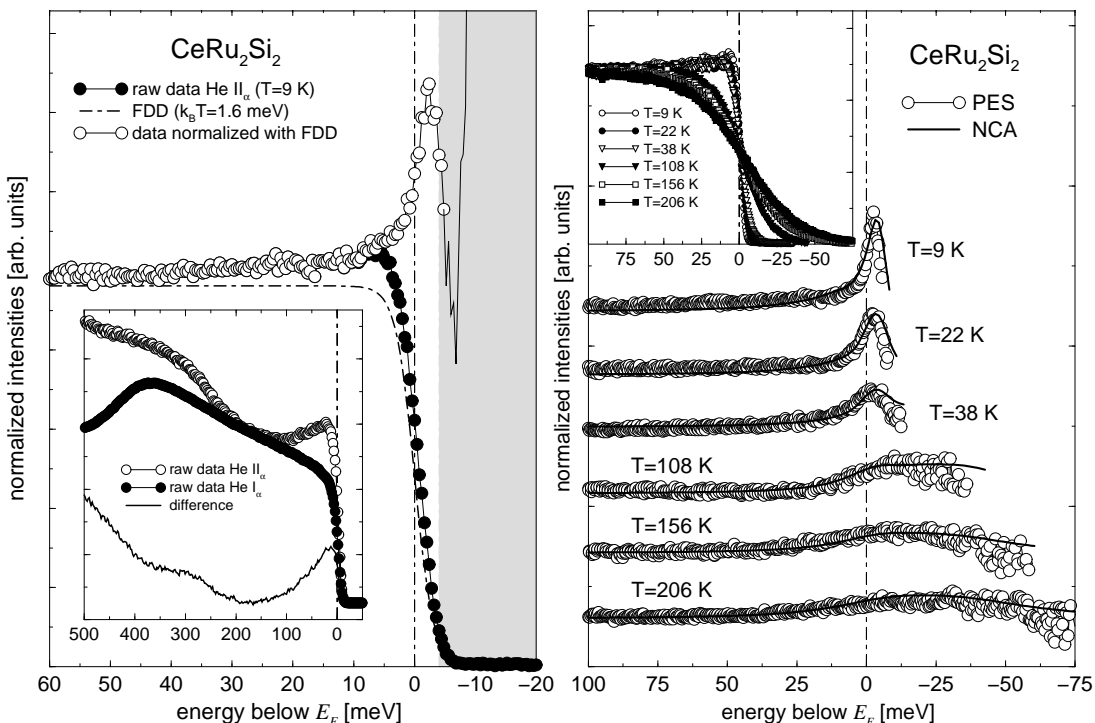


FIG. 6: Photoemission spectra of CeRu_2Si_2 (He II_α , $h\nu = 40.8$ eV). Left panel: normalization at $T = 11$ K (cf. Fig. 3); the inset shows an extended energy range ($\Delta E \approx 15$ meV) including the SO ($J = 7/2$) excitation at ≈ 290 meV below E_F taken with He II_α radiation (open circles) and with He I_α (filled circles). Right panel: temperature dependence of the experimental (He II_α) and the calculated $4f$ spectral function of CeRu_2Si_2 after the normalization. Model parameters: $\epsilon_f = -1.54$ eV, $D = 4.2$ eV, $\Delta_{CF} = 18/33$ meV, $\Delta_{SO} = 295$ meV, $V = 170$ meV. The inset shows the raw data normalized to the same intensity at a binding energy of ≈ 100 meV.

above E_F , even a two-fold fine structure in the high-temperature peak can be resolved. Both features, the CF satellite below E_F in the low-temperature data and the broad split peak at high temperatures are well described by the NCA calculation *including* the crystal field resolved degeneracy of the $4f$ levels. Without this CF splitting, there is only the spin-orbit splitting on the scale of $\Delta_{SO} = 250$ meV, which does not contribute to the investigated energy range, and the observed temperature dependence of the spectra can not be described in the SIAM quantitatively. The high spectral intensity at E_F at temperatures $T \gg T_K$ is an immediate result of the existence of the crystal field structures.

We performed analogous investigations on the HF compounds CeRu_2Si_2 , CeNi_2Ge_2 , and CeSi_2 which exhibit T_K 's in ascending order from 16 to 40 K. The results of our PES investigations are shown in Figs. 6–8. In each figure the left panel shows the analysis of the low-temperature data and the right panel gives the temperature dependence of the near- E_F spectral features. In the following we restrict ourselves to the He II_α data because all $4f$ states are much more pronounced than at low photon energies (He I). Especially in the case of the ternary Ce compounds displayed here, the intensity of the $4f$ spectral features below E_F is reduced dramatically, in

contrast to CeCu_6 for which the $4f$ features could still be observed in the He I data. Even by irradiation with He II_α the near- E_F spectra of CeRu_2Si_2 , CeNi_2Ge_2 , and CeSi_2 show only a weak $4f$ fine structure.

A comparison of the He I and He II spectra is given in the insets of Figs. 5–8. Taking the difference of the two spectra⁶⁶ is a useful method to extract the $4f$ contribution from other states near E_F . This can be particularly important, when there is a strong modulation of the non- $4f$ background intensity, which is e.g. the case for CeRu_2Si_2 and CeNi_2Ge_2 ^{47,67}. Here one has the overlap with Ru $4d$ and Ni $3d$ bands, respectively, that have a comparatively high photoemission cross-section for photon energies in the UV range.⁶⁴ In the case of CeCu_6 , CeCu_2Si_2 , and CeSi_2 the contribution of non $4f$ states in the interesting energy range is rather small and — although not negligible — without a fine structure on the scale of a few tens of meV. Another method to extract the $4f$ spectra from the net photoemission signal is *resonant photoemission spectroscopy* (RESPES) at the Ce $3d$ or $4d$ absorption edges.⁶⁸ Although this method is limited in energy resolution and therefore not suitable for investigations of the fine structure on the meV scale, the relative intensity and energetic position of the ionization peak ($4f^0$) can be investigated in detail. For all

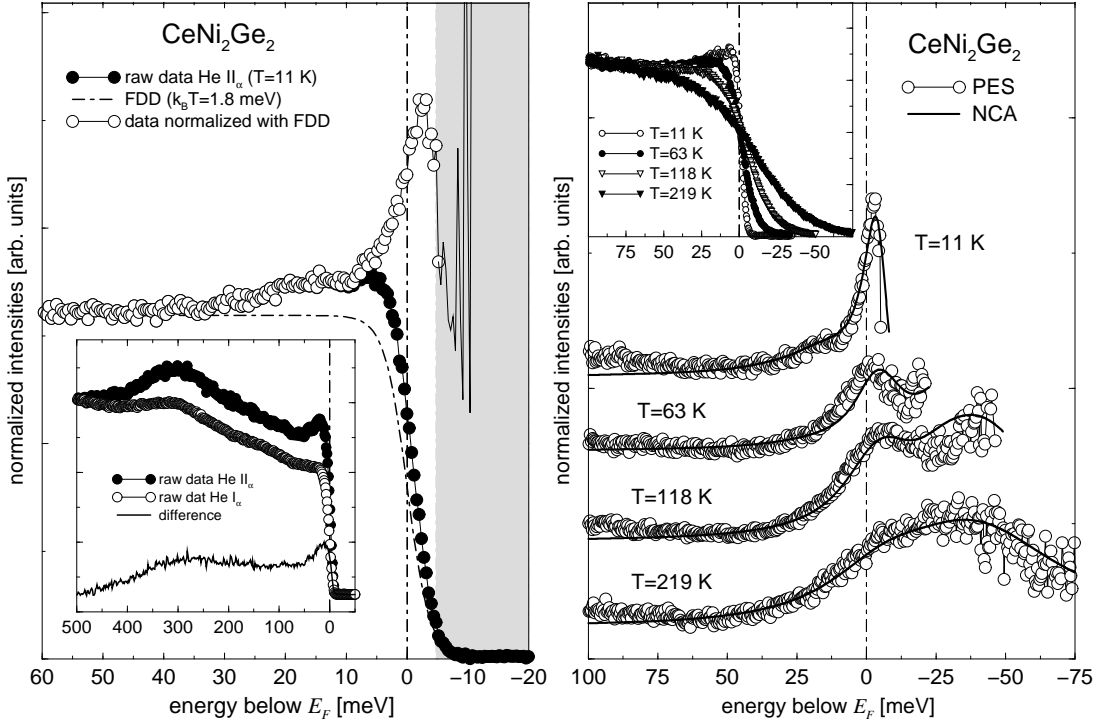


FIG. 7: Photoemission spectra of CeNi_2Ge_2 (He II_α , $h\nu = 40.8$ eV). Left panel: normalization at $T = 11$ K; the inset shows an extended energy range ($\Delta E \approx 15$ meV) including the SO ($J = 7/2$) excitation at ≈ 300 meV below E_F taken with He II_α radiation (open circles) and with He I_α (filled circles). Right panel: temperature dependence of the experimental (He II_α) and the calculated $4f$ spectral function of CeNi_2Ge_2 after the normalization. Model parameters: $\epsilon_f = -1.43$ eV, $D = 3.9$ eV, $\Delta_{CF} = 26/39$ meV, $\Delta_{SO} = 275$ meV, $V = 209$ meV. The inset shows the raw data normalized to the same intensity at a binding energy of ≈ 100 meV.

the systems measured in this work we find values for the f^0 -energy (partly from literature^{62,69,70}) that amounts to 1.7 eV, 2.6 eV, 2.2 eV, 2.2 eV, and 2.35 eV for CeCu_6 , CeCu_2Si_2 , CeRu_2Si_2 , CeNi_2Ge_2 , and CeSi_2 , respectively, similar to the values from non-resonant PES.⁶⁶ As described above, we used these values as benchmarks for the ϵ_f values in the parameter sets of the NCA calculations (see figure captions Figs. 5–8).

D. Quantitative spectral analysis: Fitting with NCA

As described in Appendix A we iteratively fit the normalized photoemission data for a quantitative data analysis. This analysis yields *one* characteristic model parameter set for each compound, which is used for the calculation of the spectra at *all* investigated temperatures. The resulting parameters are given in the captions of Figs. 5–8

In addition, each parameter set can be assigned to a certain Kondo temperature T_K , which is the Kondo temperature of the respective system. To get the T_K values we calculated the NCA spectra for each parameter set in the unitarity limit at $T = 0.1 \times T_K$. The linewidth of the Kondo resonance in this low-temperature limit defines

immediately the Kondo temperature by $\text{FWHM} \sim k_B T_K$ due to the scaling properties of the SIAM. The resulting T_K 's are given in Tab. I together with the crystal field energies Δ_{CF} and the Kondo temperatures determined from other experimental methods, i.e. INS and transport measurements. One should note that these reference bulk values are spread over a wide range, indicating some systematic uncertainties in the determination.

For all compounds we find an excellent quantitative agreement of our T_K values with the Kondo temperatures determined by INS studies.^{33,49,50,51,55,57} In addition, we find a good coincidence of the crystal field splittings for CeCu_6 , CeCu_2Si_2 and CeSi_2 with the INS values from Refs. 51,54. In the case of CeRu_2Si_2 and CeNi_2Ge_2 the CF energy separations could not be determined experimentally upto now, mainly because of uncertainties in the assignment of the CF level scheme.^{71,72} Therefore in the case of CeRu_2Si_2 we compare our values with theoretical results proposed by Zwickyagl *et al.*,⁵⁸ based on specific heat measurements⁷¹ and again we find an excellent agreement. A recent study on CeNi_2Ge_2 claims the first observation of CF structures in INS experiments on this compound, giving values that correspond rather well with our results.⁵⁹

In summary, the comparison shows that all of our re-

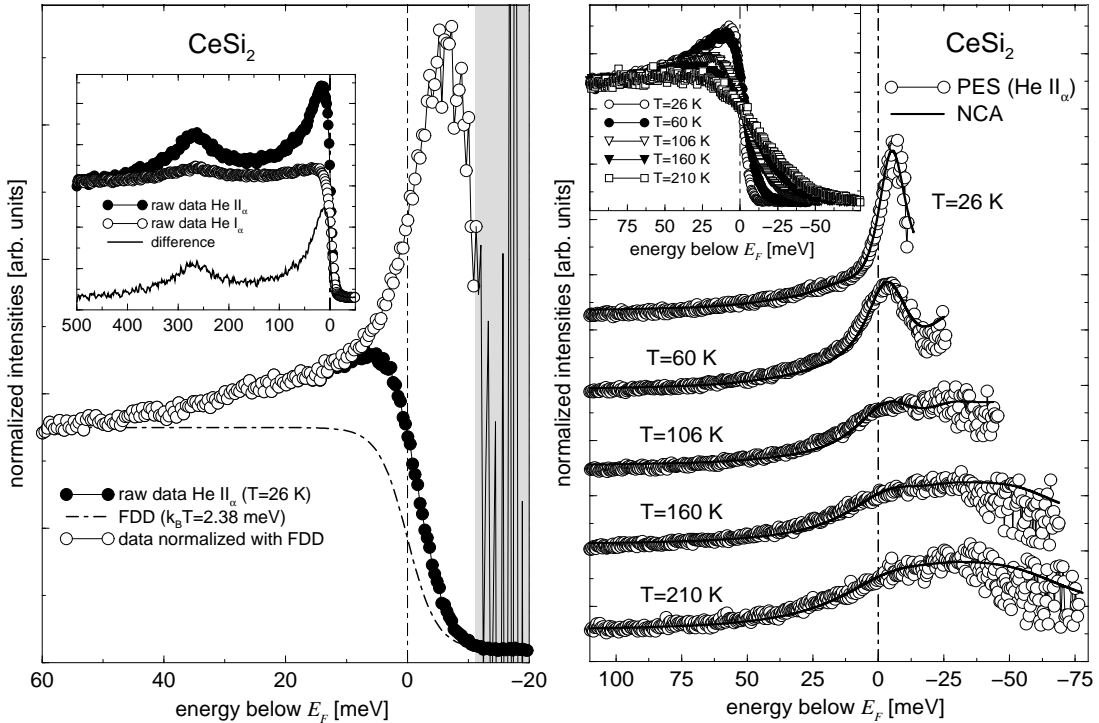


FIG. 8: Photoemission spectra of CeSi_2 (He II_{α} , $h\nu = 40.8$ eV). Left panel: normalization at $T = 11$ K; the inset shows an extended energy range ($\Delta E \approx 15$ meV) including the SO ($J = 7/2$) excitation at ≈ 280 meV taken with He II_{α} radiation (open circles) and with He I_{α} (filled circles). Right panel: temperature dependence of the experimental (He II_{α}) and the calculated $4f$ spectral function of CeSi_2 after the normalization. Model parameters: $\epsilon_f = -1.35$ eV, $D = 3.7$ eV, $\Delta_{CF} = 25/48$ meV, $\Delta_{SO} = 270$ meV, $V = 203$ meV. The inset shows the raw data normalized to the same intensity at a binding energy of ≈ 100 meV.

sults are in reasonable agreement with the values from the other methods. This is surprising because of two possible problems in our method: 1.) In contrast to transport and INS measurements is PES a *surface sensitive* technique and the surface properties of a rare-earth compound are not necessarily identical with the bulk properties, in particular the Kondo temperatures might be completely different. 2.) The SIAM, on which the NCA calculations of the spectra are based, contains several significant simplifications that might influence a quantitative description of width and position of the Kondo resonance.

Considering the first point, one has to mention that there is an ongoing debate in how far PES with excitation energies in the VUV-range will be able to reflect the *bulk properties* of Ce compounds. At these photon energies (and the respective photoelectron kinetic energies in the range of 40 eV for He II) the information depth is at a minimum of a few lattice constants.⁷³ Therefore, one performs additional photoemission measurements at higher photon energies to increase the information depth. PES with photon energies in the soft x-ray range, e.g. in resonance with the Ce $3d-4f$ absorption edge at $h\nu \approx 880$ eV, is regarded as a sufficiently bulk sensitive method with an information depth of about three times larger than

for He II.⁵² On this basis Sekiyama *et al.*^{74,75,76} have performed $3d-4f$ RESPEs studies on CeRu_2Si_2 with a noticeably high energy resolution ($\Delta E = 120$ meV). They compared the experimental spectra with results from NCA calculations, including CF splittings of 51.6 meV and 68.8 meV,⁷⁴ and found a good coincidence between the RESPEs data and the NCA spectrum. The significant difference between these crystal field energies and our values prompt us to investigate this point further. We found the following results:

- (i) If we perform NCA calculations with Sekiyama's parameter set at $T = 20$ K we find clearly separate CF peaks below and above E_F . As seen in Fig. 6 we positively cannot observe such structures below E_F in our high-resolution low-temperature spectra. In addition, these CF energies would be too large to reproduce the observed temperature dependence in Fig. 6, right panel.
- (ii) If we convolute the NCA spectra at $T = 20$ K with our parameter set (see captions Fig. 6) with a Gaussian to describe an energy resolution of $\Delta E = 120$ meV, we can reproduce Sekiyama's $3d-4f$ RESPEs spectrum with the same accuracy.

Therefore we conclude, that the RESPEs results on

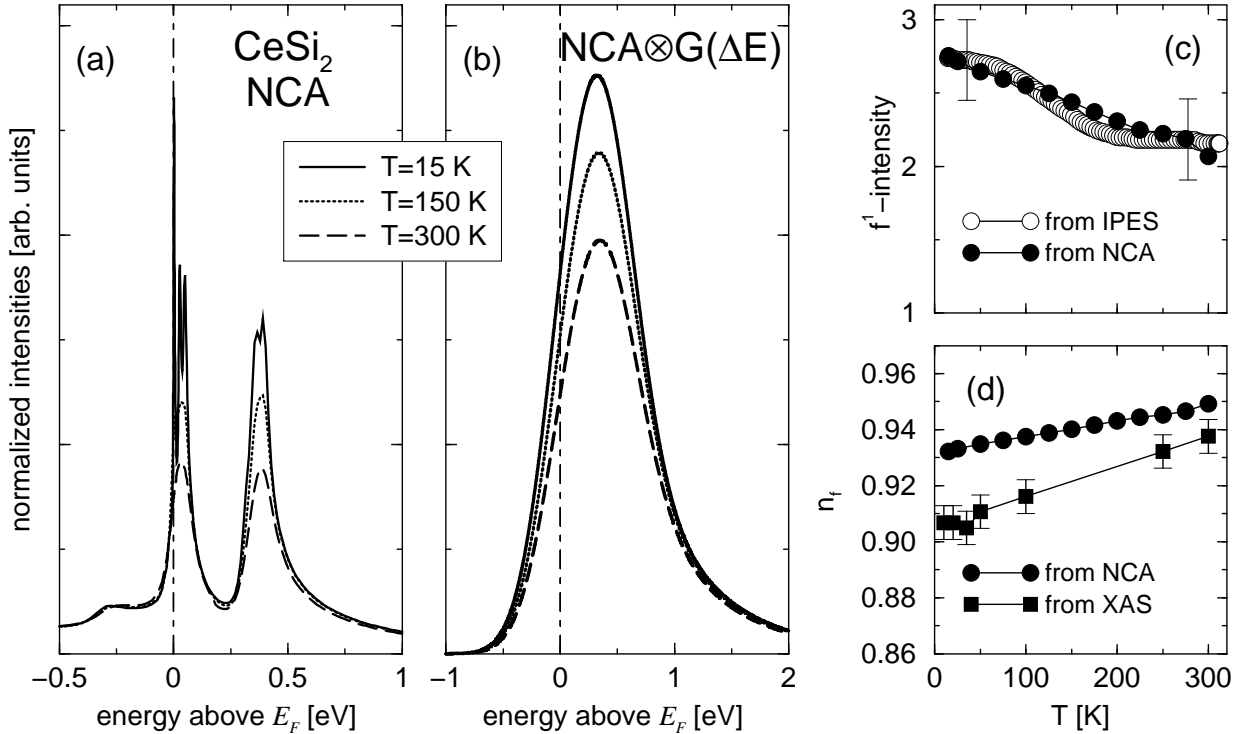


FIG. 9: Left panels: NCA spectra for CeSi_2 (parameters given in the captions of Fig. 8). (a) Raw and (b) convoluted with a Gaussian of $\text{FWHM} = 600$ meV. Panel (c) shows the (normalized) temperature dependence of the f^1 -intensity as calculated from the convoluted NCA-spectra in panel (b), in comparison with the results of IPES-studies.⁷⁷ Panel (d) shows the temperature dependence of the $4f$ occupation n_f as resulting directly from the NCA calculations. These values are compared with the ones extracted from XAS measurements at the Ce L_3 edge.⁷⁸

CeRu_2Si_2 do not contradict our results and, further more, do not indicate a quantitative deviation of the crystal field energy extracted from surface sensitive from the bulk values.

There is another possible consistence check of our analysis, using the comparison with temperature dependent (resonance) inverse photoemission spectroscopy (RIPES), which immediately has access to the spectra above the Fermi level where for Ce-systems the main spectral $4f$ weight of the Kondo resonance and its satellites appears. Again the energy resolution of this method is not sufficient to resolve the fine-structure of the $4f^1$ features, namely the Kondo resonance and its crystal field and spin-orbit satellites ($J = 7/2$). A second broad peak appears around $U - |\epsilon_f|$ and corresponds to the two-electron final state f^2 . However, the NCA spectra, which we get from our fit of the PES data, contain also the spectral information *above* the Fermi level. For the following comparison we have chosen CeSi_2 because there exist detailed RIPES⁷⁷ and x-ray absorption (XAS) investigations⁷⁸ on the temperature dependence of the $4f$ occupation number n_f , which can be determined from the intensity ratio of the f^1 and f^2 features.

To get this temperature dependence from our results we model the inverse photoemission spectra by a convolution of the NCA spectrum (with parameters from fitting

the PES data) above the Fermi level (i.e. $s(E, T) \times [1 - f(E, T)]$ at the respective temperature, cf. Appendix A) with a Gaussian describing the finite energy resolution of the RIPES experiment. The maximum position and the line width of the result — including Kondo resonance, CF satellites and spin-orbit ($J = 7/2$) partner — are identical to the experimental values within the experimental errors.⁷⁷ The left two panels of Fig. 9 shows (a) the un-broadened NCA spectra at three different temperatures and (b) the result of the convolution ($\Delta E = 600$ meV). From this modeled RIPES spectrum we take the temperature dependent integrated intensity for a comparison with the experimental temperature dependence.

Panel (c) of Fig. 9 gives the temperature dependence of the relative integrated RIPES intensities $I(f^1)/I(f^2)$ of CeSi_2 published in Ref. 77 (open circles). This intensity ratio, proportional to $1 - n_f$, clearly increases at low temperatures and the curve even suggests the existence of the plateaus well above and below $T_K \approx 30$ K as expected from the theory. We compare this behavior with the integrated intensity from Fig. 9 (b), scaled linearly to match the RIPES value at the minimum temperature of 15 K (there is no f^2 peak since $U_{ff} = \infty$ in our model). A clear coincidence of the two results is obvious, in particular if one takes the error bars of the RIPES experiment into account. However, the S -shape of the experimental

temperature dependence is less pronounced.

From an analysis of the NCA spectra one can also immediately determine the $4f$ occupation number n_f . Experimentally, this $4f$ occupation can be measured by x-ray absorption spectroscopy (XAS), e.g. at the Ce L_3 edge at $h\nu \approx 5720$ eV. Although this method is truly bulk sensitive, one has to know that the final state consists of an additional electron in the $5d$ valence states, which can lead to a slightly modified (final state) $4f$ occupation sampled by this method. However, Fig. 9 (d) gives the temperature dependence of n_f as extracted from an XAS experiment at the Ce L_3 edge of CeSi₂.⁷⁸ Although the shape of both curves is very similar, the XAS values are typically 0.01–0.03 smaller than the NCA numbers. The authors in Ref. 78 explain this difference by surface effects in PES, but this a) can be ruled out by our previous observations, and b) is usually exceeded by the final state effect in XAS.^{79,80} However, the qualitative agreement between XAS and PES/NCA result is reasonable and indicates that our data analysis is reliable.

Considering the surface effects in the special case of CeSi₂, which has the highest T_K of all Ce systems investigated in this work, one should note that the published Kondo temperatures, including the values from spectroscopy methods, differ significantly in a range of $T_K \approx 22$ K to 140 K;^{37,51,78,81,82} the given Kondo temperatures of the other compounds have a comparatively small scatter. This leads to the impression that CeSi₂ can be regarded as borderline system between γ -Ce- and α -Ce like materials, in which the difference between the hybridization strengths at the surface (or surface near region) and the bulk becomes evident.

V. CONCLUSIONS

In the present paper we have demonstrated that high-resolution photoemission allows a detailed and quantitative investigation of the $4f$ spectral features of low T_K cerium compounds close to the Fermi level. The Kondo resonance, which for Ce-systems has a maximum above E_F , could be restored for all investigated γ -Ce like HF systems by application of a well known normalization procedure. The resulting $4f$ spectra can be iteratively fitted by NCA calculations based on the SIAM, using individual model parameter sets including the spin-orbit and, in particular, the crystal field one-electron energies ϵ_f . Our results demonstrate that the consideration of the crystal-field splitting and the corresponding fine structure in the $4f$ spectra is of high importance for the consistency of the photoemission results with the thermodynamic properties. Surface effects can be ruled out for the investigated γ -Ce like systems. In spite of the known limitations of the model, our data analysis yields Kondo temperatures and crystal field energies that are in surprisingly good agreement with values from other experimental methods published in the literature. For the investigated temperature range, the description by a

local model — namely the SIAM — is obviously sufficient to describe the photoemission data with an energy resolution of the order of the Kondo temperature.

Acknowledgments

This work was supported by the Deutsche Forschungsgemeinschaft, grant nos. Hu 149/19-1 and Re 1469/4-3 (D.E., S.H., F.R.), through SFB 608 (J.K.) and by the Virtual Institute for Research on Quantum Phase Transitions at the University of Karlsruhe (P.W., H.v.L.). Particularly one of the authors (S.H.) thanks O. Gunnarsson for many enlightening discussions and communications over a number of years.

APPENDIX A: NORMALIZATION PROCEDURE

On the example of the $3d$ bands of Ni(111), Greber⁸³ has shown that a careful analysis of photoemission data close to the Fermi level allows an extended access to the thermally excited spectral features up to $5k_B T$ above E_F . Two conditions for this method have to be fulfilled: 1.) a satellite free and highly intense photon source must provide low noise data, and 2.) the total experimental energy resolution ΔE must be at least comparable to the thermal broadening $4k_B T$ of the Fermi edge; we meet these two conditions by using the experimental setup described above. The normalization method has been established for the qualitative spectroscopic investigation of the near- E_F range for various compounds, both for angular integrated and angular resolved data (see e.g. Refs. 20,84,85,86)

The experimental photoemission spectrum I can be described as the density of electronic states (or spectral function) $s(E, T)$ multiplied by the temperature dependent Fermi-Dirac distribution (FDD) $f(E, T)$. To consider the finite energy resolution, the product must be convoluted by the spectrometer function $g(E, \Delta E)$, which is usually approximated by a Gaussian with the full width at half maximum (FWHM) ΔE . Note that in our case the Gaussian describes nearly perfectly all reference spectra^{26,87}, independent from the individual spectrometer settings. Thus one gets the photoelectron spectrum

$$I(E, T) = [s(E, T) \cdot f(E, T)] \otimes g(E, \Delta E), \quad (\text{A1})$$

plus statistical noise, which we neglect in the following discussion (see Ref. 83 for more). In principle, this relation is also valid for angular resolved spectra, but here the finite angular resolution must be taken into account too.

The normalization procedure is realized by dividing the measured spectrum $I(E, T)$ by a Gaussian-broadened FDD:

$$\frac{[s(E, T) \cdot f(E, T)] \otimes g(E, \Delta E)}{f(E, T) \otimes g(E, \Delta E)}. \quad (\text{A2})$$

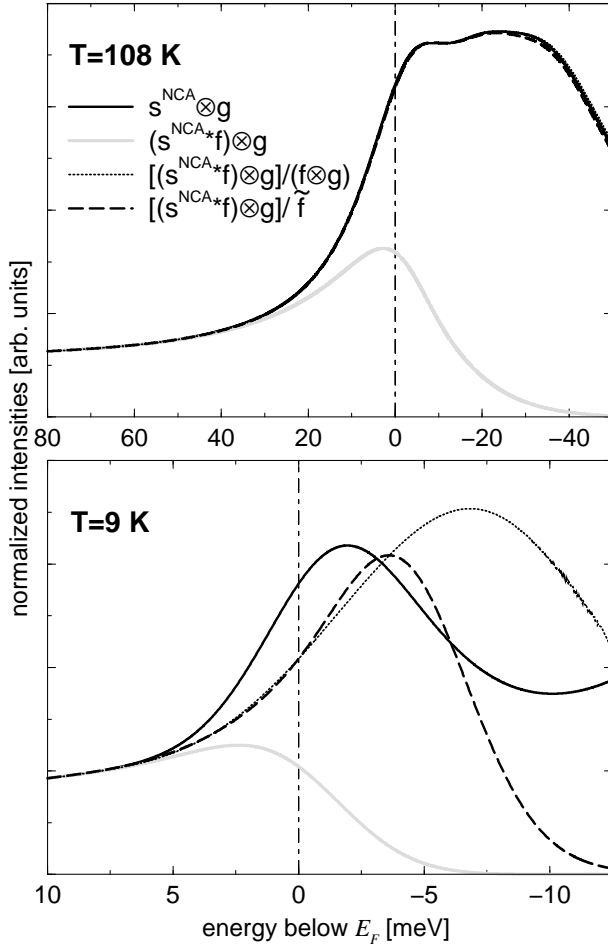


FIG. 10: Application of the normalization procedure of eq. (A2) at two different temperatures. Top panel: $T = 108 \text{ K} \gg \Delta E/k_B$, lower panel: $9 \text{ K} \ll \Delta E/k_B$. The energy resolution was $\Delta E = 5.4 \text{ meV}$. The grey curves give the modeled photoemission spectra, including FDD and Gaussian broadening, the black solid lines represent the (broadened) intrinsic spectral functions.

Because the convolution is not distributive (i.e. $[s \cdot f] \otimes g \neq [s \otimes g] \cdot [f \otimes g]$), the result of eq. (A2) is *not* equal to the broadened spectral function $s(E, T) \otimes g(\Delta E, E)$. In other words, the normalization procedure does not *a priori* reveal the intrinsic spectral function. As long as the energy broadening ΔE is small compared to the thermal

broadening $4k_B T$, the deviation between the normalization result and $s \otimes g$ is small and the result gives a useful qualitative information about the structures in the energy range up to $5k_B T$ above E_F .

However, the normalization can be used for even a *quantitative* analysis of the intrinsic spectral function when an iterative procedure is applied.²¹

The influence of this effect can be demonstrated by its application to model spectral functions (similar to the theoretical NCA spectra with realistic parameters) at different temperatures. The top panel of Fig. 10 gives the broadened intrinsic spectrum $s^{NCA} \otimes g$ with $\Delta E = 5.4 \text{ meV}$ (black solid line) and the modeled photoelectron spectrum $[s^{NCA} \cdot f] \otimes g$ according to eq. (A2) (grey line). We divide the latter by $f \otimes g$ with $T = 108 \text{ K}$ and get the dotted curve, that differs only little from the desired result $s^{NCA} \otimes g$ over the investigated temperature range of approximately up to $5k_B T$.

In this high-temperature case one can replace — as also stated in Ref. 83 — the denominator in eq. (A2), i.e. the broadened FDD $f \otimes g$, by a bare FDD $\tilde{f}(E, T_{eff})$ with an effective temperature of $T_{eff} = \sqrt{T^2 + (\Delta E/4k_B)^2}$. As shown in the top panel of Fig. 10 this simplified normalization is in good agreement with $s^{NCA} \otimes g$.

For low temperatures $T \lesssim \Delta E/k_B$, the difference between the normalized spectrum — with convoluted or effective FDD — and the intrinsic spectrum becomes significant (see lower panel of Fig. 10). Both the resulting width and the maximum position deviate considerably from the right numbers. Surprisingly, the shape of the the normalization with \tilde{f} is closer to the intrinsic spectrum $s \otimes g$ in the present case than the one with $f \otimes g$. As described above, the difference between the individual curves decreases with increasing temperature, finally matching when $T \gg \Delta E$.

However, at low temperatures the spectral shape of the normalized spectrum must not be used to determine line width and position directly. Instead one has to *fit* the spectra iteratively by comparing (e.g. by calculating χ^2) the normalized experimental data with a theoretical spectrum treated the same way. This means one has to model the experimental spectrum according to eq. A1, and use the same normalization procedure for this modeled spectrum and for the experimental data. If the curves match, one can get the position and the line width from the bare $s^{NCA}(E, T)$ included in the modeled function.

* corresponding author. Email: reinert@physik.uni-wuerzburg.de

¹ K. A. Gschneidner, Jr. and L. R. Eyring, eds., *Handbook on the physics and chemistry of rare earths* (North-Holland, Amsterdam–New York–Oxford, 1982–1999).

² F. Steglich, J. Aarts, C. D. Bredl, W. Lieke, D. Meschede, W. Franz, and H. Schäfer, *Phys. Rev. Lett.* **43**(25), 1892 (1979).

³ G. R. Stewart, *Rev. Mod. Phys.* **56**(4), 755 (1984).

⁴ G. R. Stewart, *Rev. Mod. Phys.* **73**, 797 (2001).

⁵ P. W. Anderson, *Phys. Rev.* **124**, 41 (1961).

⁶ J. Kondo, *Prog. Theor. Phys.* **32**, 37 (1964).

⁷ J. R. Schrieffer and P. A. Wolff *Phys. Rev.* **149**, 491 (1966).

⁸ O. Gunnarsson and K. Schönhammer, *Phys. Rev. B* **28**(8), 4315 (1983).

⁹ O. Gunnarsson and K. Schönhammer, *Phys. Rev. B* **31**(8),

- 4815 (1985).
- 10 R. Bulla, T. A. Costi and T. Pruschke, submitted to Rev. Mod. Phys. (), (2007); cond-mat/0701105.
 - 11 T. A. Costi, J. Kroha, and P. Wölfle, Phys. Rev. B **53**, 1850 (1996).
 - 12 N. E. Bickers, D. L. Cox, and J. W. Wilkins, Phys. Rev. B **36**(4), 2036 (1987).
 - 13 J. Kroha, P. Wölfle, and T. A. Costi, Phys. Rev. Lett. **79**, 261 (1997).
 - 14 J. Kroha and P. Wölfle, J. Phys. Soc. Jpn. **74** (1), 16 (2005).
 - 15 J. Kroha and P. Wölfle, in *Theoretical Methods for Strongly Correlated Electrons*, D. Senechal, A.-M. Tremblay, and C. Bourbonnais Eds., CRM Series in Mathematical Physics, pp. 297 (Springer, Berlin, Heidelberg, New York, 2003); cond-mat/0105491.
 - 16 F. Reinert, D. Ehm, S. Schmidt, G. Nicolay, S. Hüfner, J. Kroha, O. Trovarelli, and C. Geibel, Phys. Rev. Lett. **87**(10), 106401 (2001).
 - 17 G. Zwicknagl, Adv. in Phys. **41**(3), 203 (1992).
 - 18 M. Jarrell, Phys. Rev. B **51**(12), 7429 (1995).
 - 19 F. Reinert, D. Ehm, S. Schmidt, G. Nicolay, S. Hüfner, J. Kroha, O. Trovarelli, and C. Geibel, Phys. Rev. Lett. **87**(10), 106401 (2001).
 - 20 T. Greber, T. J. Kreutz, and J. Osterwalder, Phys. Rev. Lett. **79**(22), 4465 (1997).
 - 21 D. Ehm, F. Reinert, S. Schmidt, G. Nicolay, S. Hüfner, J. Kroha, O. Trovarelli, and C. Geibel, Physica B **312–313**, 663 (2002).
 - 22 S. Kirchner, J. Kroha, and P. Wölfle, Phys. Rev. B **70**, 165102 (2004).
 - 23 J. Kroha, S. Kirchner, G. Sellier, P. Wölfle, D. Ehm, F. Reinert, S. Hüfner, and C. Geibel, Physica E **18**(1–3), 69 (2003).
 - 24 S. Kirchner, and J. Kroha, J. Low Temp. Phys. **126**, 1233 (2002).
 - 25 F. Reinert, G. Nicolay, B. Eltner, D. Ehm, S. Schmidt, S. Hüfner, U. Probst, and E. Bucher, Phys. Rev. Lett. **85**(18), 3930 (2000).
 - 26 F. Reinert, G. Nicolay, S. Hüfner, U. Probst, and E. Bucher, J. Electron Spectrosc. Relat. Phenom. **114–116**, 615 (2001).
 - 27 F. Reinert, G. Nicolay, S. Schmidt, D. Ehm, and S. Hüfner, Phys. Rev. B **63**, 115415 (2001).
 - 28 G. R. Stewart, Z. Fisk, and M. S. Wire, Phys. Rev. B **30**(1), 482 (1984).
 - 29 W. Lieke, U. Rauchschwalbe, C. B. Bredl, F. Steglich, J. Aarts, and F. R. de Boer, J. Appl. Phys. **53**(3), 2111 (1982).
 - 30 F. Steglich, C. D. Bredl, W. Lieke, U. Rauchschwalbe, and G. Sparn, Physica B **126**, 82 (1984).
 - 31 H. Yashima and T. Satoh, Solid State Commun. **41**(10), 723 (1982).
 - 32 F. Steglich, U. Rauchschwalbe, U. Gottwick, H. M. Mayer, G. Sparn, N. Grewe, U. Poppe, and J. Franse, J. Appl. Phys. **57**(1), 3054 (1985).
 - 33 G. Knopp, A. Loidl, R. Caspary, U. Gottwick, C. D. Bredl, H. Spille, F. Steglich, and A. P. Murani, J. Magn. Magn. Mater. **74**, 341 (1988).
 - 34 L. P. Regnault, W. A. C. Erkelens, J. Rossat-Mignod, J. Flouquet, E. Walker, D. Jaccard, A. Amato, and B. Hennenion, J. Magn. Magn. Mater. **63&64**, 289 (1987).
 - 35 S. Zemirli and B. Barbara, Solid State Commun. **56**(4), 385 (1985).
 - 36 H. v. Löhneysen, H. G. Schlager, and A. Schröder, Physica B **186–188**, 590 (1993).
 - 37 H. Mori, N. Sato, and T. Satoh, Solid State Commun. **49**(10), 955 (1984).
 - 38 S. Labroo and N. Ali, J. Appl. Phys. **67**(9), 4811 (1990).
 - 39 M. J. Besnus, P. Lehmann, and A. Meyer, J. Magn. Magn. Mater. **63&64**, 323 (1987).
 - 40 P. Gegenwart, F. Kromer, M. Lang, G. Sparn, C. Geibel, and F. Steglich, Phys. Rev. Lett. **82**(6), 1293 (1999).
 - 41 T. Jarlborg, H. F. Braun, and M. Peter, Z. Phys. B **52**, 295 (1983).
 - 42 L. C. Gupta, D. E. MacLaughlin, C. Tien, C. Godart, M. A. Edwards, and R. D. Parks, Phys. Rev. B **28**(7), 3673 (1983).
 - 43 T. Fukuhara, K. Maezawa, H. Ohkuni, T. Kagayama, and G. Oomi, Physica B **230–232**, 198 (1997).
 - 44 H. Yashima, T. Satoh, H. Mori, D. Watanabe, and T. Ohtsuka, Solid State Commun. **41**(1), 1 (1982).
 - 45 H. Asano, M. Umino, Y. Onuki, T. Komatsubara, F. Izumi, and N. Watanabe, J. Phys. Soc. Jpn. **55**(2), 454 (1986).
 - 46 M. Garnier, D. Purdie, K. Breuer, M. Hengsberger, and Y. Baer, Phys. Rev. B **56**(18), R11399 (1997).
 - 47 D. Ehm, F. Reinert, G. Nicolay, S. Schmidt, S. Hüfner, R. Claessen, V. Eyert, and C. Geibel, Phys. Rev. B **64**, 235104 (2001).
 - 48 F. Reinert, R. Claessen, G. Nicolay, D. Ehm, S. Hüfner, W. P. Ellis, G.-H. Gweon, J. W. Allen, B. Kindler, and W. Assmus, Phys. Rev. B **58**, 12808 (1998).
 - 49 J. Rossat-Mignod, L. P. Regnault, J. L. Jacoud, C. Vettier, P. Lejay, J. Flouquet, E. Walker, D. Jaccard, and A. Amato, J. Magn. Magn. Mater. **76&77**, 376 (1988).
 - 50 S. Horn, E. Holland-Moritz, M. Loewenhaupt, F. Steglich, H. Scheuer, A. Benoit, and J. Flouquet, Phys. Rev. B **23**(7), 3171 (1981).
 - 51 R. M. Galera, A. P. Murani, and J. Pierre, Physica B **156&157**, 801 (1989).
 - 52 C. Laubschat, E. Weschke, C. Holtz, M. Domke, O. Strebel, and G. Kaindl, Phys. Rev. Lett. **65**(13), 1639 (1990).
 - 53 J. W. Allen, G.-H. Gweon, H. T. Schek, L.-Z. Liu, L. H. Tjeng, J.-H. Park, W. P. Ellis, C. T. Chen, O. Gunnarsson, O. Jepsen, et al., J. Appl. Phys. **87**(9), 6088 (2000).
 - 54 E. A. Goremychkin and R. Osborn, Phys. Rev. B **47**(21), 14580 (1993).
 - 55 C. D. Bredl, S. Horn, F. Steglich, B. Lüthi, and R. M. Martin, Phys. Rev. Lett. **52**(22), 1982 (1984).
 - 56 S. L. Cooper, M. V. Klein, Z. Fisk, and J. L. Smith, Phys. Rev. B **34**(9), 6235 (1986).
 - 57 A. Severing, E. Holland-Moritz, B. D. Rainford, S. R. Culverhouse, and B. Frick, Phys. Rev. B **39**(4), 2557 (1989).
 - 58 G. Zwicknagl, Adv. Phys. **41**(3), 203 (1992).
 - 59 C. D. Frost, B. D. Rainford, F. Carter, and S. S. Saxena, Physica B **276–278**, 290 (2000).
 - 60 F. Patthey, W. D. Schneider, Y. Baer, and B. Delley, Phys. Rev. B **34**(4), 2967 (1986).
 - 61 L. Schlapbach, S. Hüfner, and T. Riesterer, J. Phys. C **19**, L63 (1986).
 - 62 G. Chiaia, O. Tjernberg, L. Duò, S. De Rossi, P. Vavassori, I. Lindau, T. Takahashi, S. Kunii, T. Komatsubara, D. Cocco, et al., Phys. Rev. B **55**(15), 9207 (1997).
 - 63 D. Ehm, F. Reinert, J. Kroha, O. Stockert, and S. Hüfner, Acta Phys. Pol. B **34**, 951 (2003).
 - 64 J. Yeh and I. Lindau, At. Data Nucl. tables **32**, 1 (1985).
 - 65 S. Souma, H. Kumigashira, T. Ito, T. Sato, T. Takahashi,

- and S. Kunii, *J. Phys. Soc. Jpn.* **114–116**, 729 (2001).
- ⁶⁶ M. Garnier, K. Breuer, D. Purdie, M. Hengsberger, Y. Baer, and B. Delley, *Phys. Rev. Lett.* **78**(21), 4127 (1997).
- ⁶⁷ J. D. Denlinger, G.-H. Gweon, J. W. Allen, C. G. Olson, M. B. Maple, J. L. Sarrao, P. E. Armstrong, Z. Fisk, and H. Yamagami, *J. Electron Spectrosc. Relat. Phenom.* **117–118**, 347 (2001).
- ⁶⁸ L. Duò, *Surf. Sci. Rep.* **32**, 233 (1998).
- ⁶⁹ J. M. Lawrence, A. J. Arko, J. J. Joyce, R. I. R. Blyth, R. J. Bartlett, P. C. Canfield, Z. Fisk, and P. S. Riseborough, *Phys. Rev. B* **47**(23), 15460 (1993).
- ⁷⁰ D. H. Ehm, Ph.D. thesis, Universität des Saarlandes, Saarbrücken (2002), to be published.
- ⁷¹ B. H. Grier, J. M. Lawrence, S. Horn, and J. D. Thompson, *J. Phys.: Condens. Matter* **21**, 1099 (1988).
- ⁷² G. Knebel, C. Eggert, T. Schmid, A. Krimmel, M. Dressel, and A. Loidl, *Physica B* **230–232**, 593 (1997).
- ⁷³ S. Hüfner, *Photoelectron Spectroscopy*, vol. 82 of *Springer Series in Solid-State Sciences* (Springer-Verlag, Berlin-Heidelberg-New York, 1996).
- ⁷⁴ A. Sekiyama, K. Kadono, K. Matsuda, T. Iwasaki, S. Ueda, S. Imada, S. Suga, R. Settai, H. Azuma, Y. Onuki, et al., *J. Phys. Soc. Jpn.* **69**(9), 2771 (2000).
- ⁷⁵ A. Sekiyama, T. Iwasaki, K. Matsuda, Y. Saitoh, Y. Onuki, and S. Suga, *Nature* **403**, 396 (2000).
- ⁷⁶ S. Suga and A. Sekiyama, *J. Electron Spectrosc. Relat. Phenom.* **114–116**, 659 (2001).
- ⁷⁷ M. Grioni, P. Weibel, D. Malterre, Y. Baer, and L. Duò, *Phys. Rev. B* **55**(4), 2056 (1997).
- ⁷⁸ C. Grazioli, Z. Hu, M. Knupfer, G. Graw, G. Behr, M. S. Golden, J. Fink, H. Giefers, G. Wortmann, and K. Attenkofer, *Phys. Rev. B* **63**, 115107 (2001).
- ⁷⁹ D. Malterre, *Phys. Rev. B* **43**(2), 1391 (1991).
- ⁸⁰ J. M. Lawrence, G. H. Kwei, P. C. Canfield, J. G. DeWitt, and A. C. Lawson, *Phys. Rev. B* **49**(3), 1627 (1994).
- ⁸¹ F. Patthey, W. D. Schneider, Y. Baer, and B. Delley, *Phys. Rev. Lett.* **58**(26), 2810 (1987).
- ⁸² H. Yashima, H. Mori, T. Satoh, and K. Kohn, *Solid State Commun.* **43**(3), 193 (1982).
- ⁸³ T. Greber, T. J. Kreutz, and J. Osterwalder, *Phys. Rev. Lett.* **79**(22), 4465 (1997).
- ⁸⁴ H. Kumigashira, T. Sato, T. Yokoya, T. Takahashi, S. Yoshii, and M. Kasaya, *Phys. Rev. Lett.* **82**(9), 1943 (1999).
- ⁸⁵ T. Pillo, J. Hayoz, H. Berger, F. Lévy, L. Schlapbach, and P. Aebi, *Phys. Rev. B* **61**(23), 16213 (2000).
- ⁸⁶ F. Forster, F. Hüfner, and S. Reinert, *J. Chem. Phys. B* **108**(38), 14692 (2004).
- ⁸⁷ G. Nicolay, F. Reinert, S. Schmidt, D. Ehm, P. Steiner, and S. Hüfner, *Phys. Rev. B* **62**(3), 1631 (2000).